

# Polarimetry of Nacre in Iridescent Shells

R.A. Metzler, C. Burgess, B. Regan, S. Spano, and E.J. Galvez

Department of Physics and Astronomy, Colgate University, Hamilton, NY 13346, U.S.A.

## ABSTRACT

We investigate the light transmitted or reflected from nacre (mother of pearl) taken from the iridescent shell of the bivalve *Pinctada fucata*. These nacre surfaces have a rich structure, composed of aragonite crystals arranged as tablets or bricks, 5  $\mu\text{m}$  wide and 400-500 nm thick, surrounded by 30nm thick organic mortar. The light reflected from these shell surfaces, or transmitted through thin polished layers, is rich in its polarization content, exhibiting a space dependent variation in the state of polarization with a high density of polarization singularities. Our goal is to use the polarization information to infer the structure of the biominerals and the role of the organic layer in determining the orientation of the crystals. In the experiments we send the light from a laser with a uniform state of polarization onto the shell, and analyze the light that is either transmitted or reflected, depending on the type of experiment, imaging it after its passage through polarization filters. We use the images from distinct filters to obtain the Stokes parameters, and hence the state of polarization, of each image point. We also construct the Mueller matrix for each imaged point, via 36 measurements. We do this for distinct physical and chemical treatments of the shell sample. Preliminary data shows that the organic layer may be responsible for organizing a multi-crystalline arrangement of aragonite tablets.

**Keywords:** Imaging polarimetry of nacre-sections of bivalve iridescent shells

## 1. INTRODUCTION

Light's polarization plays an intimate and subtle role in how nature functions. Organisms such as bees,<sup>1</sup> locusts, crickets<sup>2,3</sup> and damselfish<sup>4</sup> are known to use polarization states of light to navigate by ocularly detecting particular states of polarization, while other organisms such as the lookdown fish manipulate the polarization states of light for the purpose of camouflage.<sup>5</sup> The polarization of natural light is transformed when the light interacts with inorganic natural materials, such as birefringent minerals, air molecules, dust; and structured organic surfaces, such as the skin of other animals and plants. Imaging technology, which has made tremendous advances in the last fifty years, has largely ignored polarization. Cameras and detectors convey polarization-insensitive information resulting in the loss of a lot of information that we could be acquiring.<sup>6</sup> The advent of versatile polarization-sensitive imaging devices in conjunction with imaging polarimetry will enhance remote sensing, allowing a wealth of new information to become available.<sup>7</sup> It will open a new view into the subtle ways in which the natural world interacts with the environment via polarization. Imaging polarimetry is a growing technique that extracts information from an object that interacts strongly with polarization.<sup>8</sup>

Here we investigate through polarimetry the structure and composition of a complex biomaterial: the iridescent shell of a pearl oyster. The pearl oyster, *Pinctada fucata*, shown in Fig. 1 (a) and (b), is a marine bivalve (two shells joined by a natural hinge) whose shells surround the organism, primarily providing protection, amongst other functions. Each shell is composed of two distinct calcium carbonate layers, the prismatic, outer layer made of calcite prisms, and the inner, iridescent, nacre layer formed of distinct aragonite crystals, which are biaxially birefringent. The nacre layer is structured like a brick wall with 400-nm thick  $\times$  5- $\mu\text{m}$  wide inorganic aragonite bricks spaced by 30 nm thick organic mortar.<sup>9,10</sup> The aragonite crystals (bricks) are arranged in a close-packing regular arrangement. The regular structure of the layers separated by about the wavelength of visible light is responsible for the iridescence of the shell, in analogy to thin-film interference or Bragg scattering.<sup>11</sup> In the crystal layers of *Pinctada fucata*, and other bivalves, the bulk of the nacreous aragonite crystals are organized such that their optic  $c$ -axes are perpendicular to the shell surface and their optic  $a$ - and  $b$ -axes are aligned from

---

Further author information: (Send correspondence to E.J.G.)  
E.J.G.: E-mail: egalvez@colgate.edu, Telephone: 1 315 228 7205  
Proceedings of SPIE **9187**, 918704 1-11 (2014).

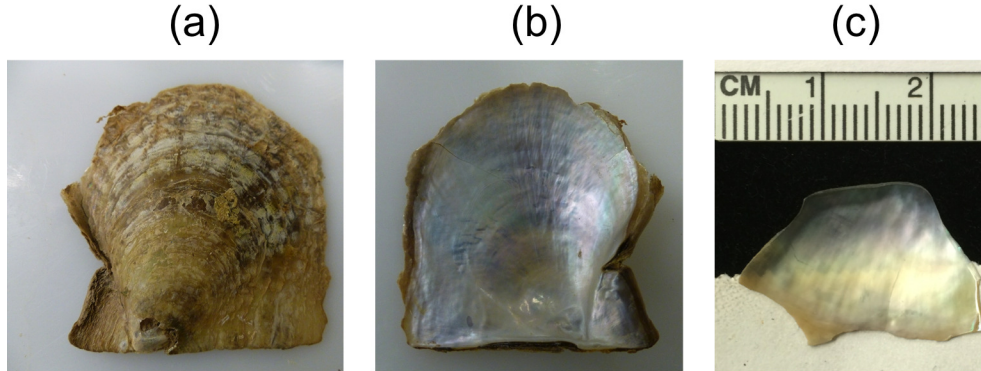


**Figure 1.** Image of the pearl oyster *Pinctada fucata*, showing the prismatic side (a), nacre side (b) and a closeup of one of the samples used in transmission experiments.

tablet to tablet.<sup>12</sup> In addition to the brick and mortar components, recent studies found evidence of organic material located within each individual aragonite brick, though the exact location of the organic material within the aragonite crystals is unknown.<sup>13</sup> The formation mechanism is a complex self-assembly process in which organic elongated proteins such as chitin likely facilitate the conversion of amorphous calcium carbonate to aligned crystalline aragonite tablets.<sup>14</sup>

Here we exploit the information that can be obtained through polarimetry to explore the structure of the iridescent nacre layer in *Pinctada fucata*, finding that the intact shell, containing both organic and mineral components, affects the polarization of transmitted light differently than a shell in which the organics have been removed. The preliminary results that we present here indicate polarimetry may be a technique that not only will be useful for studying complex optical patterns but also for examining shells. We hope that this technique, whose development is ongoing, may be able to determine the location of the organics within the individual nacre bricks, thereby answering a long-standing question in the biomineralization field.

## 2. EXPERIMENTAL METHODS

There were two components to our methods: sample preparation and polarimetry analysis. As the shells have two distinct layers, we will refer to the “inner surface” as the surface facing the mollusk, and the “outer surface” the one facing the external environment. Internal surfaces uncovered after slicing and polishing will be referred to as “bulk surfaces.” In general, nacre is composed of ordered aragonite crystals at the inner surface. This structure is increasingly misaligned further away from the inner surface, in the bulk, all the way up to the boundary with a prismatic layer, made of calcite crystals.<sup>9, 12, 15</sup> The latter extends all the way to the outer surface of the shell. To make systematic measurements, we cut and polished thin sections of nacre for analysis. Our analysis had three components: imaging polarimetry using laser light, optical microscopy, and scanning electron microscopy. We detail the methods employed in the following sections.

### 2.1. Sample preparation

The *Pinctada fucata* oysters were purchased in bulk from cnepearls.com, which sent them vacuum-sealed. Each sample was prepared by breaking a piece off the *Pinctada fucata* shell, cleaning the piece with ethanol, and polishing it to the correct thickness (about 0.3-0.5 mm). One of the samples we used for the data presented in this article is shown in Fig. 1(c). Note that the transparency of the sample is evident by its distinct brightness with black and white backgrounds. Samples were prepared to either leave the inner surface intact or lightly polished, while the bulk side of all samples were polished by hand on silicon papers lubricated with deionized water, beginning with a 600 grit and ending with a 1200 grit. The objective of polishing the bulk side was two-fold: to eliminate the prismatic layer and to thin the nacre layer to an appropriate thickness. Following the 1200 grit, the sample was polished with a nylon pad and 50-nm alumina slurry until all scratches were removed, as observed with an optical microscope at 100× magnification, shown in Fig. 2. The sample was subsequently

cleaned with ethanol and deionized water. One notices rough terraces in the inner surface of the sample, shown in Fig. 2(a). The bulk surface, shown in Fig. 2(b), reveals smoother terraces. Upon closer inspection with greater magnification, the undefined boundary of the terraces at the inner surface is due to individual aragonite tablets that are not fully close-packed, showing an intermediate step in the nacre formation.

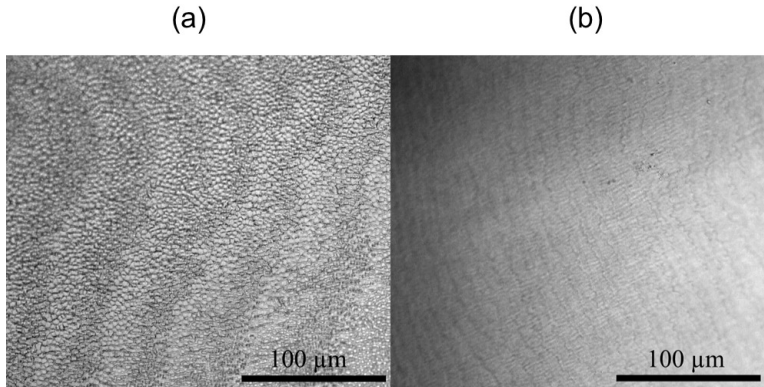


**Figure 2.** Image of a polished sample of nacre taken with an optical microscope. It shows the lightly polished inside (a) and the heavily polished bulk side (b).

For polarimetry experiments, the sample was either mounted in a padded alligator clip or on double stick tape such that the area of interest was illuminated by the laser beam. For many of the samples the mount was designed to have two distinct positions, providing two sample regions that could be selected for data collection. For at least two samples, the sample without organics was prepared following data acquisition on the intact sample by bleaching the sample while it remained mounted, thus enabling us to return to the exact same positions at which the intact sample was measured. For all samples in which the organics were removed, the sample was bleached for 72 hours and then rinsed with deionized water to remove any organic residues. Following bleaching, data was acquired in either the same two positions or in the same approximate position as for the intact shell, depending on how the sample was mounted.

## 2.2. Imaging polarimetry

A general schematic of our apparatus is shown in Fig. 3. Light from a helium-neon laser is expanded to a beam spot of 1.05 mm. With the aid of polarization elements, the beam was polarized in any of six states of polarization: linear horizontal (H), linear vertical (V), linear diagonal (D:  $45^\circ$  to the horizontal, going counter-clockwise looking into the beam), linear antidiagonal (A:  $-45^\circ$  to the horizontal, going clockwise looking into the beam), right circular (R), or left circular (L). In the forward direction the light passes neutral density filters, and is focused onto the sample with a converging lens. We used lenses with distinct focal lengths, but in this work we report on the case where the focal length was 7.4 cm. It produced a beam waist of about  $14.1 \mu\text{m}$ , illuminating about 27,000 tablets with the sample of Fig. 1(c). Past the sample we had a recollimating lens. The light beam then passed through an arrangement of waveplates and a polarizer that filtered the light in any of the 6 polarization states mentioned above. The images were collected with a digital camera.

We also measured the light reflected from the sample, and did polarimetry in the same way as in the transmissive mode. This was done by placing a non-polarizing beam splitter before the lens focusing on the sample. This way the light retroreflected by the sample was diverted at 90-degrees from the incoming beam axis for polarimetry analysis. Alternatively, with the beam splitter in place, a camera was added to observe the spot where the laser passed through the sample.

In polarimetry, the Stokes parameters are obtained by:

$$S_0 = I_H + I_V \quad (1)$$

$$S_1 = I_H - I_V \quad (2)$$

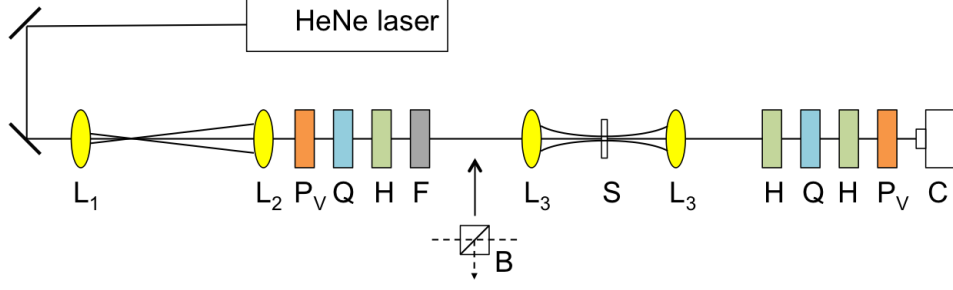


**Figure 3.** Schematic of the apparatus. Optical elements include lenses (L), polarizers with transmission axis vertical ( $P_V$ ), quarter-wave plates (Q), half-wave plates (H), and a digital camera (C). The light was focused onto a thin (0.2 mm) sample (S). We alternatively analyzed the reflection by introducing a beam splitter (B) and moving the detection filters and camera to the output port of the beam splitter.

$$S_2 = I_D - I_A \quad (3)$$

$$S_3 = I_R - I_L \quad (4)$$

Where  $I_H$ ,  $I_V$ ,  $I_D$ ,  $I_A$ ,  $I_R$  and  $I_L$  are the intensities measured with the filters H, V, D, A, R and L, respectively. The normalized Stokes parameters are:

$$s_0 = 1 \quad (5)$$

$$s_1 = S_1/S_0 \quad (6)$$

$$s_2 = S_2/S_0 \quad (7)$$

$$s_3 = S_3/S_0 \quad (8)$$

We did two types of analysis: Imaging polarimetry and Mueller polarimetry. In the first one we sent linearly polarized light in specific orientations and analyzed the polarized output via polarimetry. The specific orientations were taken relative to a measured optical axis of the sample. The latter was determined by placing the sample within two cross polarizers, and rotating the polarizers rigidly (i.e., maintaining their relative orthogonality) until the light going through was extinguished. This defined the optic axis of the sample.

The polarization ellipse consists of an ellipse of ellipticity given by

$$\epsilon = \tan \alpha = \pm \frac{b}{a}, \quad (9)$$

where  $a$  and  $b$  are the semi-major and semi-minor axes of the ellipse, respectively, and

$$\alpha = \frac{1}{2} \sin^{-1} \frac{s_3}{\sqrt{s_1^2 + s_2^2 + s_3^2}}. \quad (10)$$

We note that when  $\sqrt{s_1^2 + s_2^2 + s_3^2} \leq 1$  the light is partially polarized. The orientation of the ellipse's semi-major axis is given by

$$\theta = \frac{1}{2} \tan^{-1} \left( \frac{s_2}{s_1} \right) \quad (11)$$

The Mueller polarimetry method rests on the Mueller matrix. It is defined as:

$$M = \begin{pmatrix} m_{11} & m_{12} & m_{13} & m_{14} \\ m_{21} & m_{22} & m_{23} & m_{24} \\ m_{31} & m_{32} & m_{33} & m_{34} \\ m_{41} & m_{42} & m_{43} & m_{44} \end{pmatrix}. \quad (12)$$

**Table 1.** Matrix elements of the Mueller matrix expressed in terms of the measured coefficients. The first and second subindices in the terms (e.g.,  $I_{HH}$ ) represent the state of the incoming and detection polarization, respectively.

$m_{11}$	$m_{12}$	$m_{13}$	$m_{14}$
$\frac{1}{2}(I_{HH} + I_{HV} + I_{VH} + I_{VV})$	$\frac{1}{2}(I_{HH} + I_{HV} - I_{VH} - I_{VV})$	$\frac{1}{2}(I_{AH} + I_{AV} - I_{DH} - I_{DV})$	$\frac{1}{2}(+I_{LH} + I_{LV} - I_{RH} - I_{RV})$
$m_{21}$	$m_{22}$	$m_{23}$	$m_{24}$
$\frac{1}{2}(I_{HH} - I_{HV} + I_{VH} - I_{VV})$	$\frac{1}{2}(I_{HH} - I_{HV} - I_{VH} + I_{VV})$	$\frac{1}{2}(I_{AH} - I_{AV} - I_{DH} + I_{DV})$	$\frac{1}{2}(I_{LH} - I_{LV} - I_{RH} + I_{RV})$
$m_{31}$	$m_{32}$	$m_{33}$	$m_{34}$
$\frac{1}{2}(I_{HA} + I_{VA} - I_{HD} - I_{VD})$	$\frac{1}{2}(I_{HA} - I_{HD} - I_{VA} + I_{VD})$	$\frac{1}{2}(I_{AA} - I_{AD} - I_{DA} + I_{DD})$	$\frac{1}{2}(I_{LA} - I_{LD} - I_{RA} + I_{RD})$
$m_{41}$	$m_{42}$	$m_{43}$	$m_{44}$
$\frac{1}{2}(I_{HL} - I_{HR} + I_{VL} - I_{VR})$	$\frac{1}{2}(I_{HL} - I_{HR} - I_{VL} + I_{VR})$	$\frac{1}{2}(I_{AL} - I_{AR} - I_{DL} + I_{DR})$	$\frac{1}{2}(I_{LL} - I_{LR} - I_{RL} + I_{RR})$

The measured elements were obtained by relations listed in Table 1. They are consistent with previous work,<sup>16,17</sup> but distinct in the definitions of the state of polarization: looking into the beam as opposed to looking along the direction of the beam. Obtaining the Mueller matrix involved taking 36 measurements: six polarization filters for the six input states of polarization of the laser beam.

As discussed later, correlations between matrix elements can be used to evaluate the effect of the shell on the polarization of the light. We placed particular attention on the relations that define a single crystal retarder, of retardation  $\delta$  and with optic axis aligned by an angle  $\theta$ . The corresponding matrix is given by<sup>18</sup>

$$W_{\delta,\theta} = \begin{pmatrix} 1 & 0 & 0 & 0 \\ 0 & \cos^2 2\theta + \cos \delta \sin^2 2\theta & \sin 2\theta \cos 2\theta (1 - \cos \delta) & -\sin 2\theta \sin \delta \\ 0 & \sin 2\theta \cos 2\theta (1 - \cos \delta) & \sin^2 2\theta + \cos \delta \cos^2 2\theta & \cos 2\theta \sin \delta \\ 0 & \sin 2\theta \sin \delta & -\cos 2\theta \sin \delta & \cos \delta \end{pmatrix}. \quad (13)$$

Alternatively, a rotator with circular retardance has a matrix

$$R = \begin{pmatrix} 1 & 0 & 0 & 0 \\ 0 & \cos 2\theta & -\sin 2\theta & 0 \\ 0 & \sin 2\theta & \cos 2\theta & 0 \\ 0 & 0 & 0 & 1 \end{pmatrix}, \quad (14)$$

where  $\theta$  is the rotation angle. In the analysis that follows we try to correlate the measured matrix with specific birefringent optical operations described by the previous two matrices.

### 3. RESULTS

We performed experiments on two types of samples: polished but in its natural state, and the same sample after bleaching.

#### 3.1. Unbleached Samples

We used sample thicknesses that varied from 150  $\mu\text{m}$  to 500  $\mu\text{m}$  and found that the light transmission from samples with thicknesses up to about 400  $\mu\text{m}$  showed surprising uniformity. Thicker samples gave images with increasing non-uniform polarization. Figure 4 shows two examples of the cases where the polarization was uniform. We have plotted the image of the beam of light, following our past experience imaging space-variant optical beams.<sup>19,20</sup> The images are color-coded with the orientation of the semi-major axis of the polarization ellipse at each point in the beam. In the figure, teal-cyan is vertical at 0, blue-purple is  $+45^\circ$  (counter-clockwise

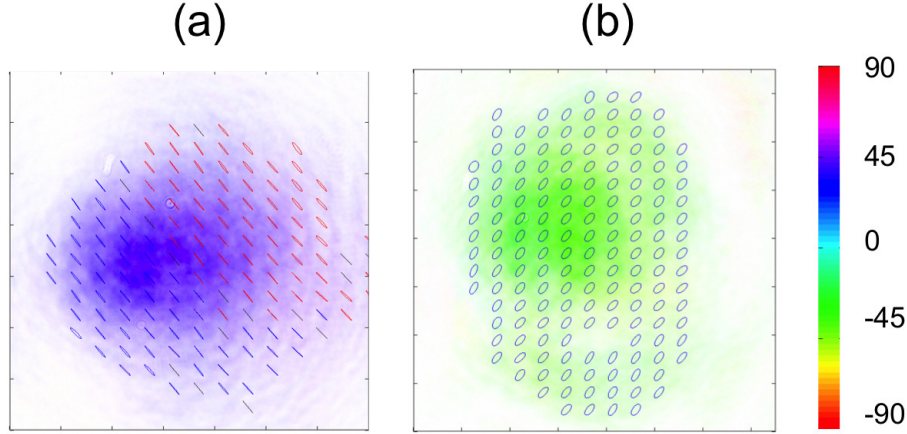


**Figure 4.** Two images of the space-variant polarization of the light with constant input state that was: (a) linearly polarized  $45^\circ$  clockwise to vertical, and (b) linearly polarized horizontally. Both images are of locations in the sample of Fig. 1(c). The color encodes the orientation of the semimajor axis of the polarization ellipse, and the saturation encodes the total intensity. The color of the drawn states of polarization reflect the handedness of the state: red for right-handed and blue for left-handed.

from vertical), green is  $-45^\circ$  (clockwise from vertical) and red is horizontal ( $\pm 90^\circ$ ). At periodic intervals, and when the intensity of the light exceeds 10% of the maximum intensity we plot the polarization ellipse at that point. The color of the ellipses represents the handedness: red for right-handed and blue for left-handed.

The sample data shown in Fig. 4 involved transmission through two locations of the same sample of thickness  $200 \pm 40 \mu\text{m}$ . The regularity of the polarization of the output is quite remarkable, especially considering that the light is traversing a *tens of thousands* of aragonite tablets. Thus, these tablets must be naturally arranged with a remarkable degree of alignment. The input state of polarization of the image of Fig. 4(a) was linear anti-diagonal ( $A$ ;  $45^\circ$  counter-clockwise to the vertical). We see that the output is indeed close to the input alignment, forming an average angle of  $40 \pm 2$  with the vertical. Further analysis with other input orientations of linear polarization showed that this location behaved like a polarization rotator. That is,  $\theta_{\text{out}} = (1.01 \pm 0.04)\theta_{\text{in}} - (5.4 \pm 1.1)$  (in degrees), which rotates the input polarization by  $-5.4^\circ$ .

It is important to note that the sample did not behave fully like a monolithic single crystal. Notice in Fig. 4(a) that the polarization throughout the beam is mostly linear, but with a finite ellipticity with an average value of  $\epsilon_{\text{av}} = 0.025 \pm 0.069$ . However, over half of the sample the slight ellipticity is left-handed (blue) and the other half is right-handed (red). This difference became more visible when the input polarization was circular, where the difference in the state of polarization between the two halves was more pronounced.

We tested the input-output alignment of the polarization through other locations of other samples. The two cases that we illustrate in Fig. 5 correspond to distinct locations on the same sample (not the one in Fig. 1(c)). One case (squares) yielded rotation, with  $\theta_{\text{out}} = (0.97 \pm 0.12)\theta_{\text{in}} - (34 \pm 5)$  (in degrees), which imply a rotation by  $-34^\circ$ . In the other case of Fig. 5 (diamonds), the sample behaved like a flipper, or half-wave plate, giving  $\theta_{\text{out}} = (-1.02 \pm 0.08)\theta_{\text{in}} - (84 \pm 8)$  (in degrees). The unit-negative slope is indicative of flipping about an axis, which in this case was  $8^\circ$  from the vertical. The error bars on the square (diamond) symbols represent the standard deviation with about 84,000 (31,000) pixels of data. The case of Fig. 4(b) is more indicative of the general transformation of the polarization.

To get more complete information about the effect of the shells we obtained the Mueller matrix for the two cases (a) and (b) of Fig. 4, which are shown in Figs. 6 and 7, respectively. We calculated the average value of the center portion of the matrix elements (about 70,000 pixels) to enable quantitative analysis of the data. The

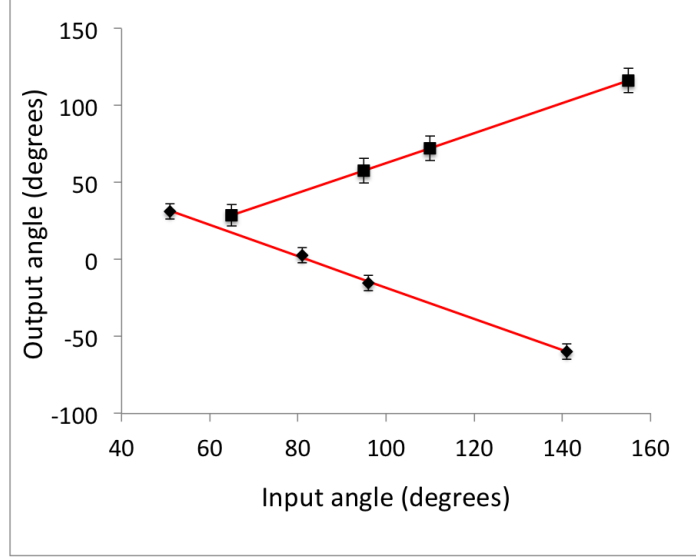


**Figure 5.** Data showing measured average orientations of the semi-major axes of the polarization ellipses as a function of the input linear polarization angle. The two sets of data correspond to cases where the sample rotated (squares) or flipped (diamonds) the input polarization orientation. Solid lines are fits to the data.

measured matrices for these reduced portions of the images are:

$$M_{\text{loc-1}} = \begin{pmatrix} 1.00 & 0.03 \pm 0.05 & 0.02 \pm 0.04 & 0.04 \pm 0.16 \\ 0.03 \pm 0.05 & 0.87 \pm 0.08 & -0.20 \pm 0.03 & 0.19 \pm 0.13 \\ 0.01 \pm 0.03 & 0.14 \pm 0.04 & 0.83 \pm 0.10 & 0.27 \pm 0.21 \\ -0.03 \pm 0.03 & 0.03 \pm 0.10 & 0.01 \pm 0.08 & -0.67 \pm 0.13 \end{pmatrix} \quad (15)$$

and

$$M_{\text{loc-2}} = \begin{pmatrix} 1.00 & 0.00 \pm 0.08 & -0.01 \pm 0.07 & 0.02 \pm 0.09 \\ 0.02 \pm 0.06 & -0.18 \pm 0.08 & -0.81 \pm 0.06 & 0.45 \pm 0.07 \\ 0.01 \pm 0.08 & -0.58 \pm 0.06 & 0.46 \pm 0.07 & 0.62 \pm 0.07 \\ 0.01 \pm 0.09 & 0.79 \pm 0.08 & 0.11 \pm 0.09 & 0.54 \pm 0.09 \end{pmatrix}. \quad (16)$$

These matrices were obtained using Table 1. The elements were normalized to element  $m_{11}$ , which is 1 by definition. The matrices indeed show the complexity of the samples, while they also show a surprising regularity. Should a sample be a retarder, then following Eq. 13 we should expect a matrix of the form:

$$M_{\text{ret}} = \begin{pmatrix} 1 & 0 & 0 & 0 \\ 0 & a & b & -c \\ 0 & b & a' & d \\ 0 & c & -d & e \end{pmatrix}, \quad (17)$$

where the symbols represent numbers between  $-1$  and  $1$ . Similarly, a rotator, would have a matrix of the form

$$M_{\text{rot}} = \begin{pmatrix} 1 & 0 & 0 & 0 \\ 0 & a & b & 0 \\ 0 & -b & a & 0 \\ 0 & 0 & 0 & 1 \end{pmatrix}, \quad (18)$$

As can be seen by Fig. 6 and Eq. 15, the first case seems to behave mostly as a rotator (Eqs. 14 and 18): elements  $m_{22} = m_{33}$  within the uncertainty, and  $m_{23} \sim -m_{32}$ . The actual values yield distinct rotations, but simply reading the values off would mean we are oversimplifying the effect of the sample too much. In the

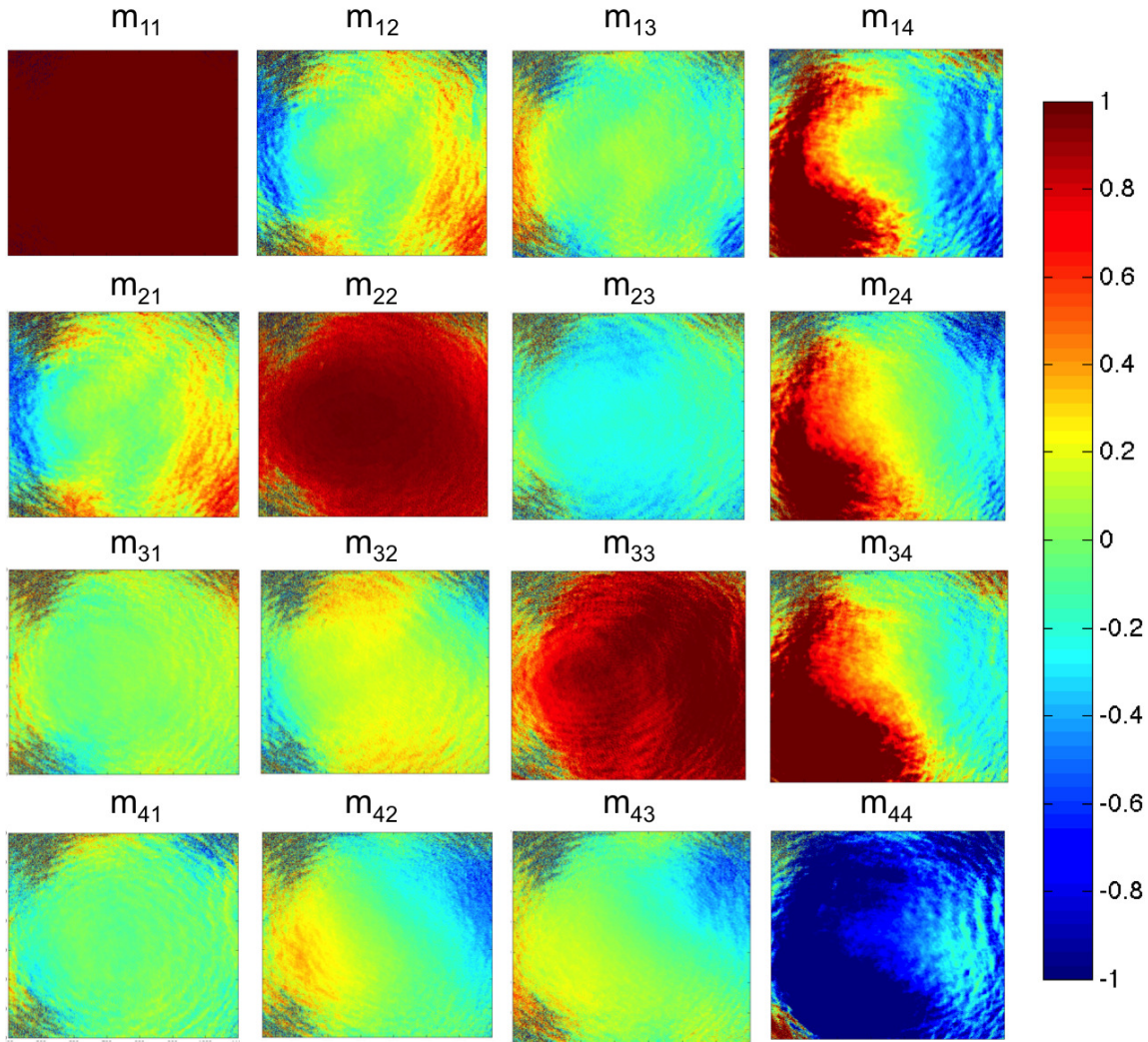


**Figure 6.** Measured images of the Mueller matrix elements corresponding to the case of Fig. 4(a).

analysis of the change in the input/output ellipse orientation we ignored the change in ellipticity. Another telling clue of the complexity is that  $m_{44}$  is distinct from 1, the expectation, well beyond uncertainty. The case of Fig. 7 and Eq. 16 is more indicative of a retarder: we see that  $m_{12} = m_{13} = m_{14} = m_{21} = m_{31} = m_{41} = 0$  to within their respective uncertainties, and similarly  $m_{23} = m_{32}$ . However, it is also the case that  $m_{24} \neq -m_{42}$  and  $m_{34} \neq -m_{43}$ , contrary to what we expect from a monolithic retarder. The latter point is the key: we are comparing an assembly of tens of thousands of retarders, arranged by an organic self assembly, with a monolithic inorganic one. While previous studies have shown that within a layer and even across several layers the crystal tablets are aligned, the alignment is imperfect, especially when taken across several layers, as we are examining here.

### 3.2. Bleaching

In addition to examining intact nacre layers, we conducted polarimetry experiments on samples before and after bleaching. Bleaching is known to remove inter-crystalline organic molecules that are present in biomineral samples<sup>13,21</sup> and thus the bleached samples are those in which the organic matrix surrounding the nacre tablets has been removed. As shown in Fig. 8, when bleached, the uniformity and order observed in the polarimetry of the intact samples no longer exists. The data acquired from the bleached samples, both at the same exact

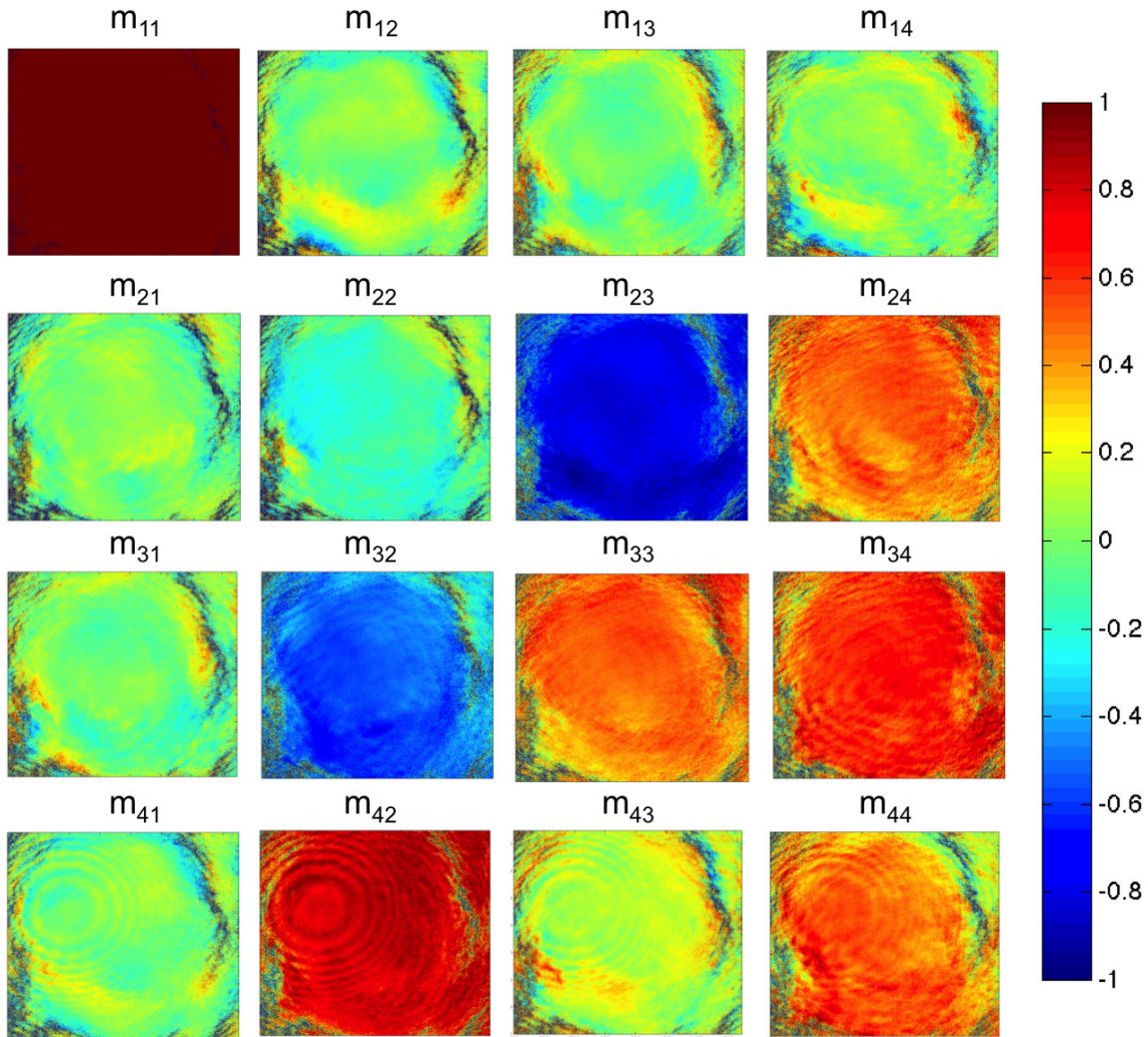


**Figure 7.** Measured images of the Mueller matrix elements corresponding to the case of Fig. 4(b).

location as the data acquired on intact samples and in different regions, indicates that the organic matrix plays an important role in maintaining the orientation and organization of the individual nacre tablets even after nacre formation.

This observation is confirmed by examining bleached and unbleached samples with a scanning electron microscope (SEM), as shown in Fig. 9. The nacre tablets of the bleached sample are separated from one another and space can be seen in between each of the tablets. In the unbleached sample, the individual tablets are difficult to differentiate from one another because they form a continuous layer with the organic matrix acting as the mortar that holds the tablets close to one another and in place. It was also observed that upon bleaching, the sample lost its iridescent sheen, as shown at the bottom of Fig. 9.

#### 4. CONCLUSIONS

In summary, we performed an optical polarimetry study of sections of nacre taken from a *Pinctada fucata* bivalve shell. The transmitted light reveals the birefringent nature of nacre, but also its surprising regularity. When subject to bleaching, most of the order, as determined through polarimetry, disappears. Scanning-electron images confirm the distinct structure of the sample when the organic mortar in between the tablets is dissolved

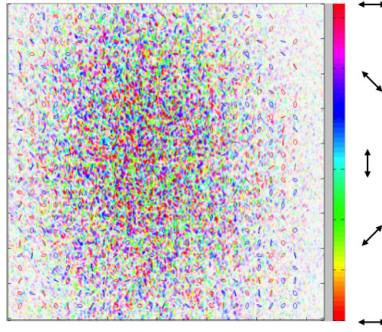


**Figure 8.** Polarimetry of a sample that was bleached. Color indicates the orientation of the semimajor axis of the polarization ellipses.

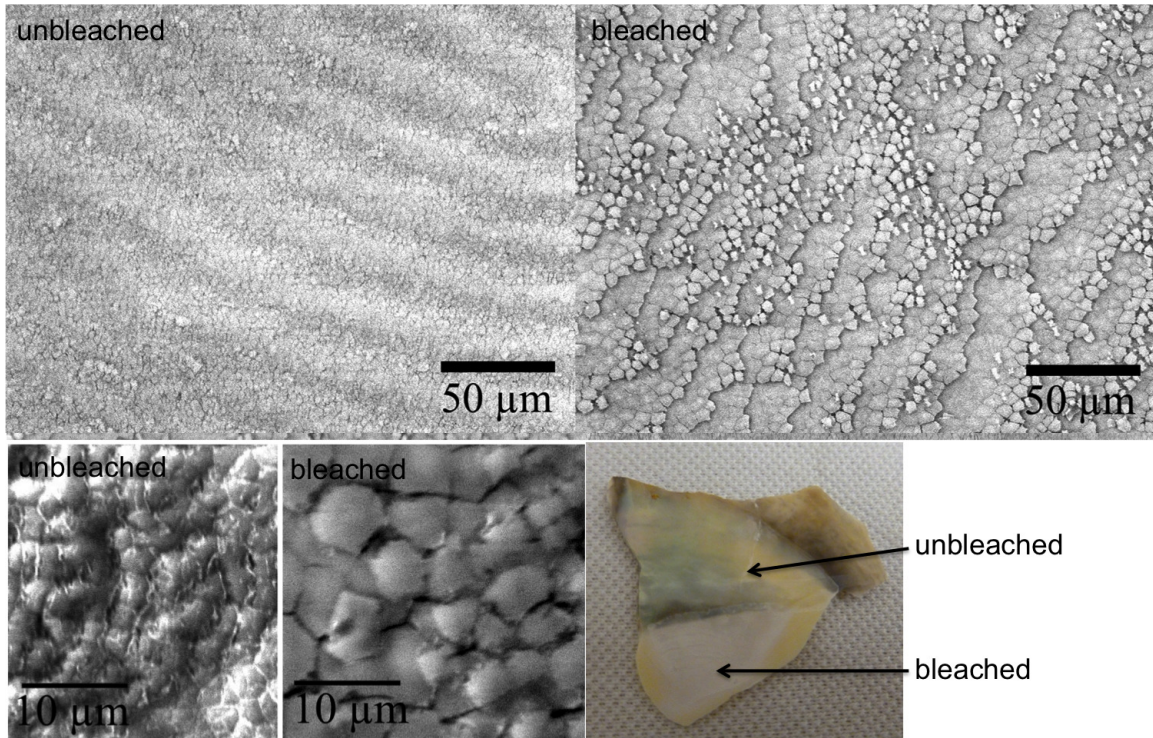


**Figure 9.** Scanning-electron microscope images of bleached and unbleached samples (top and bottom left, with distinct resolutions, and in full-size sample (about 2-3 cm across).

and removed. The bleaching action produces a significant scatter due to the gaps that appear in between the aragonite tablets.

This work represents a sample of a program that we have just begun. It is a unique type of research that uses optical polarimetry to inquire about the structure of nacre. As we refine our methods we expect to get a better understanding of the structure of aragonite crystals in nacre and the role of the organic matter that is laid out alongside, and perhaps within, inorganic aragonite tablets.

## 5. ACKNOWLEDGMENTS

This work was funded by the Picker Interdisciplinary Science Institute of Colgate University.

## REFERENCES

1. Rossel, S., and Wehner, R. "Polarization vision in bees," *Nature* **323**, 129-131 (1986).
2. Srinivasan, M. V. "Honeybees as a model for the study of visually guided flight, navigation, and biologically inspired robotics," *Physiol. Rev.* **91**, 413-460 (2011).
3. Labhart, T. , "Polarization-opponent interneurons in the insect visual system," *Nature* **331**, 435-437 (1988).
4. Mussi, M. and Haimberger, T. J. and Hawryshyn, C. W. , "Behavioural discrimination of polarized light in the damselfish *Chromis viridian* (family Pomacentridae)," *J. Exp. Biol.* **208**, 3037-3046 (2005).
5. Brady, P. C. and Travis, K. A. and Maginnis, T. and Cummings, M. E. , "Polaro-cryptic mirror of the look down as a biological model for open ocean camouflage," *Proc. Nat. Acad. of Sci. U.S.A.* **110**, 9764-9769 (2013).
6. Tyo, J.S., Goldstein, D.L., Chenault, D.B., and Shaw, J.A., "Review of passive imaging polarimetry for remote sensing applications," *Appl. Opt.* **45**, 5453-5469 (2006).
7. Miller, D.A. and Dereniak, E.L., "Selective polarization imager for contrast enhancements in remote scattering media," *Appl. Opt.* **51**, 4092-4102 (2012).
8. Pierangelo, A., Benali, A., Antonelli, A.-R., Novikova, T., Validire, P., Gayet, B. and De Martino, A., "*Ex-vivo* characterization of human colon cancer by Mueller polarimetric imaging," *Opt. Express*, **19**, 1582-1593 (2011).
9. Gilbert, P. U. P. A. and Metzler, R. A. and Zhou, D. and Scholl, A. and Doran, A. and Young, A. and Kunz, M. and Tamura, N. and Coppersmith, S. N. , "Gradual ordering in red Abalone nacre," *J. of Am. Chem. Soc.* **130**, 17519-17527 (2008).
10. Levi-Kalisman, Y. and Falini, G. and Addadi, L. and Weiner, S. , "Structure of the nacreous organic matrix of a bivalve mollusk shell examined in the hydrated state using cryo-TEM," *J. Struct. Biol.* **135**, 8-17 (2001).
11. Liu, Y. and Shigley, J. E. and Hurwit, K. N. , "Iridescence color of a shell of the mollusk *Pinctada Margaritifera* caused by diffraction," *Opt. Express* **4**, 177-182 (1999).
12. Checa, A. G. and Rodriguez-Navarro, A. B. , "Self-organisation of nacre in the shells of Pterioidea (Bivalvia: Mollusca)," *Biomaterials* **26**, 1071-1079 (2005).
13. Pokroy, B. and Quintana, J. P. and Caspi, E. N. and Berner, A. and Zolotoyabko, E. , "Anisotropic lattice distortions in biogenic aragonite," *Nat. Mater.* **3**, 900-90 (2004).
14. Addadi, L. and Joester, D. and Nudelman, F. and Weiner, S. , "Mollusk shell formation: a source of new concepts for understanding biomineralization processes," *Chem. Eur. J.* **12**, 980-987 (2006).
15. Metzler, R. A. and Abrecht, M. and Olabisi, R. M. and Ariosa, D. and Johnson, C. J. and Frazer, B. H. and Coppersmith, S. N. and Gilbert, P. U. P. A. , "Architecture of columnar nacre, and implications for its formation mechanism," *Phys. Rev. Lett.* **98**, 268102 (2007).
16. Bickel, W.S. and Bailey, W.M., "Stokes vectors, Mueller matrices, and polarized scattered light," *Am. J. Phys.* **53**, 468-478 (1985).
17. Hielscher, A.H., Eick, A.A., Mourant, J.R., Shen, D., Freyer, J.P., and Bigio, I.J., "Diffuse backscattering Mueller matrices of highly scattering media," *Opt. Express* **1**, 441-453 (1997).
18. Chipman, R.A., "Polarimetry," in *Handbook of Optics, Volume II*, Bass, M., Van Stryland, E.W., Williams, D.R., and Wolfe W.L. Eds. (McGraw-Hill Inc., New York, 1995).
19. Galvez, E.J., Khadka, S., Schubert, W.H., and Nomoto, S., "Poincaré-beam patterns produced by non-separable superpositions of LaguerreGauss and polarization modes of light," *Appl. Opt.* **51**, 2925-2934 (2012).
20. Galvez, E.J., Rojec, B.L., Kumar, V., and Viswanathan, N.K., "Generation of isolated asymmetric umbilics in light's polarization," *Phys. Rev. A* **89**, 031801 1-4 (2014).
21. Ramos-Silva, P. and Marin, F. and Kaandrop, J. and Marie, B. , "Biomineralization toolkit: The importance of sample cleaning prior to the characterization of biomineral proteomes," *Proc. .Nat. Acad. Sci. U.S.A.* **110**, 2144-2146 (2013).